IEEE Access
Multidisciplinary | Rapid Review | Open Access Journal

Received March 31, 2022, accepted April 17, 2022, date of publication April 18, 2022, date of current version April 27, 2022.

Digital Object Identifier 10.1109/ACCESS.2022.3168707

Robust CFAR Detector With Ordered Statistic of Sub-Reference Cells in Multiple Target Situations

TAEHEE JEONG[1], SUNGYEONG PARK[2], JEONG-WOOK KIM[1], AND JONG-WON YU[1], (Member, IEEE)

[1]School of Electrical Engineering, Korea Advanced Institute of Science and Technology (KAIST), Yuseong-gu, Daejeon 34141, Republic of Korea
[2]Radar and EW Technology Center, Agency for Defense Development (ADD), Daejeon 34186, Republic of Korea

Corresponding author: Jong-Won Yu (drjwyu67@kaist.ac.kr)

ABSTRACT Herein, a robust constant false alarm rate (CFAR) detector with ordered statistic of sub-reference cells (OSS-CFAR) is proposed in multiple target situations. This detector can improve background level estimation and reduce computational complexity using sub-reference cells. The detection performance of the OSS-CFAR detector and of conventional CFAR detectors in multiple target situations are investigated and compared using computer simulations and experimental data with sea clutter. The simulations and experimental results show that the OSS-CFAR detector achieves robust detection performance with low computational complexity, whereas conventional CFAR detectors suffer performance degradation in multiple target situations. At the clutter edge, the OSS-CFAR detector with appropriate parameters achieves an acceptable false alarm rate compared to conventional CFAR detectors.

INDEX TERMS Constant false alarm rate detector, clutter edge, multiple target situations, ordered statistic of sub-reference cells.

I. INTRODUCTION

Constant false alarm rate (CFAR) detectors are important for use in modern radar systems because they automatically calculate a detection threshold in unknown backgrounds (noise plus clutter) to detect the presence of targets [1]– [7]. Cell averaging CFAR (CA-CFAR) detector [8], [9] adaptively calculates the detection threshold using the mean power of the reference cells around the cell under test (CUT) and multiplies it by a scale factor that depends on the required false alarm rate. The CA-CFAR detector is based on two assumptions [8]. First, the reference cells contain background with the same statistics as the CUT, so that they are representative of the background. Second, the reference cells do not contain any targets, so that they only have backgrounds of noise and clutter. Under these conditions, the background statistics in the CUT can be estimated from the measured range and Doppler reference cells in pulsed Doppler radar.

With real radar systems, since the targets on the ground and the sea can be dense and the clutter is complex, the background includes multiple targets and clutter edges. For example, when an airborne radar steers a highway, it is often the case that there are tens of interfering targets, since the signal of vehicle targets can be received from several tens of kilometers on the ground. Unfortunately, in multiple target situations, the CA-CFAR detector suffers from poor detection performance due to the high detection threshold caused by the targets in the reference cells. This is called the masking effect. Moreover, at the clutter edge, the CA-CFAR detector increases false alarms because there is a difference in power distribution between the reference cells. Therefore, the detection threshold is often lower than the CUT which has high power at the clutter edge [10].

To overcome these performance degradations in multiple target situations and the clutter edge, several CFAR detectors have been proposed. These are the smallest of cell averaging CFAR (SOCA-CFAR) detector [11], the greatest of cell averaging CFAR (GOCA-CFAR) detector [11], [12], and the ordered statistic CFAR (OS-CFAR) detector [13]. The SOCA-CFAR detector and the OS-CFAR detector were proposed to solve the masking effect caused by interfering targets in the reference cells. The performance of the SOCA-CFAR detector and the OS-CFAR detector is better than that of the CA-CFAR detector in multiple target

The associate editor coordinating the review of this manuscript and approving it for publication was Brian Ng.

situations, but the SOCA-CFAR detector and the OS-CFAR detector still have false alarms at the clutter edge and poor detection performances when many interfering targets exist in the reference cells. The OS-CFAR detector requires prior information about the number of the interfering targets in order to remove all interfering targets from the reference cells. This limitation degrades the detection performance in the absence of prior information. The GOCA-CFAR detector was proposed to avoid false alarms at the clutter edge. The GOCA-CFAR detector achieves a good false alarm rate at the clutter edge. However, the GOCA-CFAR detector shows performance degradation in multiple target situations due to the masking effect.

In recent years, to improve detection performance in multiple target situations and the clutter edge, many CFAR detectors have been studied based on weighted iteration [14], [15], machine learning [16], [17], variability index [18], and outlier rejection based on the Grubbs criterion [19]. These studies have improved detection performances in multiple target situations and the clutter edge. However, with the methods using iteration [14], [15], [18], [19], since the convergence time depends on the initial value and the number of iterations, the convergence time can increase depending on the situation. This limitation is critical for real-time radar systems. In addition, the machine learning method [16], [17] has performance differences depending on the training data. If the detector receives an input that differs from the previously learned data, performance degradation occurs.

In this paper, a robust CFAR detector with ordered statistic of sub-reference cells (OSS-CFAR) is proposed to improve the detection performance in multiple target situations and the clutter edge. To overcome performance degradation in these cases, we grouped the reference cells into sub-reference cells and set guard cells with the same range and the same Doppler as the CUT. The detection performances of the proposed OSS-CFAR detector and the conventional CFAR detectors in multiple target situations and the clutter edge were investigated and compared using computer simulations and experimental data with sea clutter. Since the conventional CFAR detectors, such as the CA-, SOCA-, GOCA-, and OS-CFAR detectors, are commonly used in airborne and maritime radars, these detectors are compared with the proposed detector. In multiple target situations, the OSS-CFAR detector achieves robust detection performance with low computational complexity, whereas conventional CFAR detectors suffer performance degradation. The computer simulation results and experimental results show that the OSS-CFAR detector is effective in multiple target situations and achieves an acceptable false alarm rate at the clutter edge.

The contributions of our work are summarized as follows. First, we proposed a robust CFAR detector with low computational complexity compared to the conventional CFAR detectors in multiple target situations and the clutter edge. Therefore, the OSS-CFAR detector can be applied to radar systems that require real-time processing. Second, we achieved good performance CFAR detector that does not require prior information about the number of interfering targets in the reference cells. The OS-CFAR detector requires prior information about the number of the interfering targets in the reference cells, but the OSS-CFAR detector does not require prior information. Although there are several CFAR detectors that do not require prior information, the OSS-CFAR detector has a clear advantage over the others because it operates robustly in multiple target situations without any prior information. Finally, the proposed OSS-CFAR detector is useful in practical multiple target situations. We applied the proposed CFAR detector and the conventional CFAR detectors to experimental data with multiple targets and sea clutter. The experimental results show that the OSS-CFAR detector is effective in multiple target situations with an unknown information about the number of the interfering targets.

The remaining parts of this paper are organized as follows. In Section II, we introduce the conventional CFAR detectors and explain the relationships between the false alarm rate and scale factor. The proposed OSS-CFAR detector is presented in Section III. We describe the detection scheme in Section III-A, the false alarm rate in Section III-B, and the computational complexity in Section III-C. In Sections IV and V, the advantages of the OSS-CFAR detector in multiple target situations and a clutter edge are verified and analyzed using simulation results and experimental results. Finally, we conclude this paper with a brief summary in Section VI.

II. CONVENTIONAL CFAR DETECTORS

In this section, the conventional CFAR detectors (CA-, SOCA-, GOCA-, and OS-CFAR) are described. The CFAR detectors can be performed in a one-dimensional range axis or two-dimensional range Doppler map [8]. With the aforementioned CFAR detectors, we assumed the two-dimensional range Doppler map data as the input and passed it through the square-law detector, allowing the signals in the range Doppler map to have power values. Two-dimensional windows of the CFAR detectors are provided in Fig. 1. The red cell is the CUT, the yellow cells are guard cells, and the blue cells are reference cells. The bold lines in the figure indicate the boundary of the reference cells. Detection threshold calculations associated with target detection are covered in detail in the following subsections.

The power sample $X(i, j)$ at i-th range axis and j-th Doppler axis of range Doppler map in Fig. 1 is assumed to follow an exponential distribution, which is commonly used to describe the noise power distribution in radar systems. The probability density function (PDF) could be expressed as

$$f_X(x) = \frac{1}{2\sigma^2} \exp\left(-\frac{x}{2\sigma^2}\right) \tag{1}$$

where x denotes the power of the sample and σ denotes the distribution parameter. The detection scheme and the false alarm rate of the CFAR detectors are described in the following subsections.

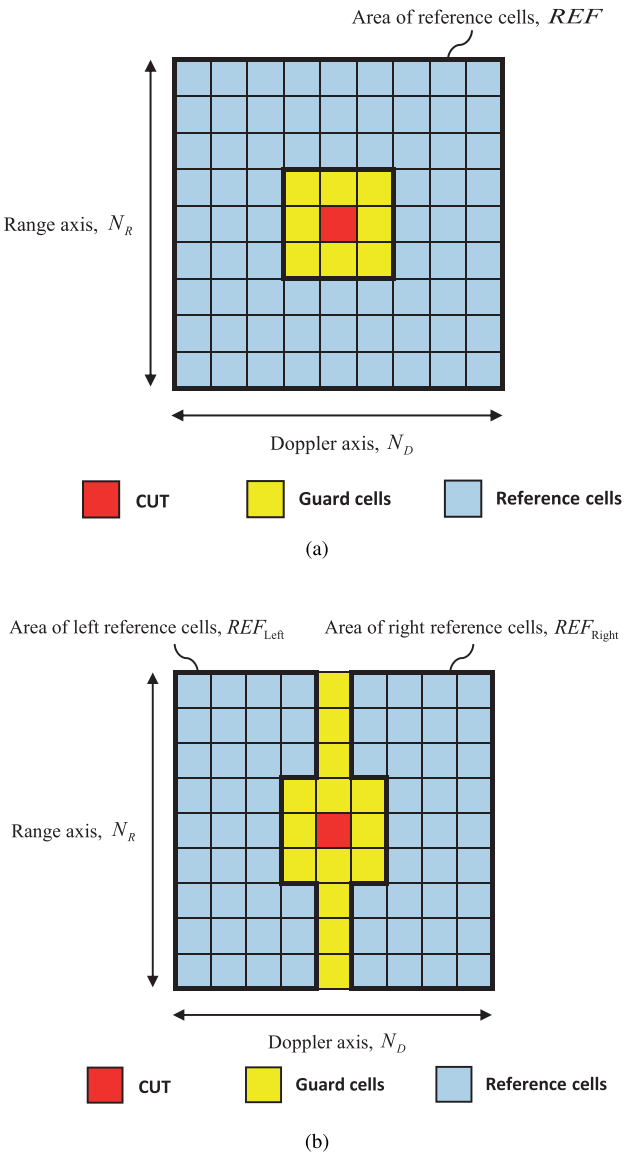

FIGURE 1. Two-dimensional window of the conventional CFAR detectors: (a) CA-CFAR and OS-CFAR, (b) SOCA-CFAR and GOCA-CFAR.

A. CELL AVERAGING CFAR

The CA-CFAR detector estimates the background level by the sum of the powers in the reference cells, as shown in Fig. 1(a), as

$$\beta_{\text{CA}} = \sum_{i,j \in REF} X(i,j) \tag{2}$$

where REF denotes the area of the reference cells.

In the CA-CFAR detector, the false alarm rate $P_{\text{fa,CA}}$ is

$$P_{\text{fa,CA}} = (1+\alpha_{\text{CA}})^{-N} \tag{3}$$

where N denotes the number of reference cells and α_{CA} denotes a scale factor [20]. The detection threshold is defined as the product of the estimated background level and the scale factor. Therefore, the detection threshold of the CA-CFAR detector is

$$T_{\text{CA}} = \alpha_{\text{CA}}\beta_{\text{CA}} \tag{4}$$

B. SMALLEST OF CELL AVERAGING CFAR

The SOCA-CFAR detector estimates the background level by selecting the minimum of the two power sum values calculated in the left and right reference cells, as shown in Fig. 1(b), as

$$\beta_{\text{SOCA}} = \min(U, V) \tag{5}$$

where U and V are as follows.

$$U = \sum_{i,j \in REF_{\text{Left}}} X(i,j) \tag{6}$$

$$V = \sum_{i,j \in REF_{\text{Right}}} X(i,j) \tag{7}$$

where REF_{Left} and REF_{Right} denote the area of the left and the right reference cells, respectively. In the SOCA-CFAR detector, the false alarm rate $P_{\text{fa,SOCA}}$ is

$$P_{\text{fa,SOCA}} = \left(\frac{2}{(2+\alpha_{\text{SOCA}})^{\frac{N}{2}}}\right) \sum_{q=0}^{\frac{N}{2}-1} \binom{\frac{N}{2}-1+q}{q} (2+\alpha_{\text{SOCA}})^{-q} \tag{8}$$

where N denotes the number of reference cells and α_{SOCA} denotes the scale factor [11]. The detection threshold of the SOCA-CFAR detector is

$$T_{\text{SOCA}} = \alpha_{\text{SOCA}}\beta_{\text{SOCA}} \tag{9}$$

C. GREATEST OF CELL AVERAGING CFAR

The GOCA-CFAR detector estimates the background level by selecting the maximum of the two power sum values calculated in the left and right reference cells, as shown in Fig. 1(b), as

$$\beta_{\text{GOCA}} = \max(U, V) \tag{10}$$

where U and V are as (6) and (7), respectively.

In the GOCA-CFAR detector, the false alarm rate $P_{\text{fa,GOCA}}$ is

$$\frac{P_{\text{fa,GOCA}}}{2} = (1+\alpha_{\text{GOCA}})^{-\frac{N}{2}} - (2+\alpha_{\text{GOCA}})^{-\frac{N}{2}} \times \sum_{q=0}^{\frac{N}{2}-1} \binom{\frac{N}{2}-1+q}{q} (2+\alpha_{\text{GOCA}})^{-q} \tag{11}$$

where N denotes the number of reference cells and α_{GOCA} denotes the scale factor [11]. The detection threshold of the GOCA-CFAR detector is

$$T_{\text{GOCA}} = \alpha_{\text{GOCA}}\beta_{\text{GOCA}} \tag{12}$$

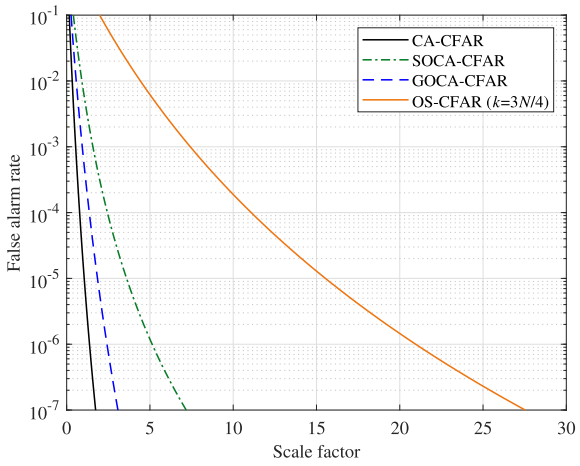

FIGURE 2. False alarm rates of the conventional CFAR detectors according to the scale factor when N is 16 and k is 12.

D. ORDERED STATISTIC CFAR

The OS-CFAR detector estimates the background level by selecting the k-th sample in ascending order in the reference cells as shown in Fig. 1(a), as

$$\beta_{\mathrm{OS}} = X_{(k)}, \quad k \in 1, 2, \cdots, N \tag{13}$$

where $X_{(k)}$ are as follows.

$$X_{(1)} \leq X_{(2)} \leq \cdots \leq X_{(N)} \tag{14}$$

where N denotes the number of reference cells. A value of $k = 3N/4$ is appropriate for practical application [13].

In the OS-CFAR detector, the false alarm rate $P_{\mathrm{fa,OS}}$ is

$$P_{\mathrm{fa,OS}} = k\binom{N}{k}\frac{\Gamma(\alpha_{\mathrm{OS}} + N - k + 1)\Gamma(k)}{\Gamma(\alpha_{\mathrm{OS}} + N + 1)} \tag{15}$$

where $\Gamma(\cdot)$ denotes the gamma function and α_{OS} denotes the scale factor [13]. The detection threshold of the OS-CFAR detector is

$$T_{\mathrm{OS}} = \alpha_{\mathrm{OS}}\beta_{\mathrm{OS}} \tag{16}$$

E. RELATIONSHIPS BETWEEN THE FALSE ALARM RATE AND SCALE FACTOR OF CONVENTIONAL CFAR DETECTORS

The relationships between the false alarm rate and scale factor of the conventional CFAR detectors described so far are illustrated in Fig. 2 as examples. In this figure, the number of reference cells is 16 and the background level representative value k of the OS-CFAR detector is 12.

In Fig. 2, the false alarm rate decreases as the scale factor increases for all CFAR detectors. This is because the detection threshold increases as the scale factor increases. Accordingly, the increasing detection threshold reduces the false alarm rate due to noise or clutter. Using Fig. 2, it is possible to obtain the required scale factor for the desired false alarm rate. For example, if the desired false alarm rate is 10^{-3}, the scale factors of the CA-, SOCA-, GOCA-, and OS-CFAR detectors are 0.54, 1.573, 0.934, and 7.42, respectively.

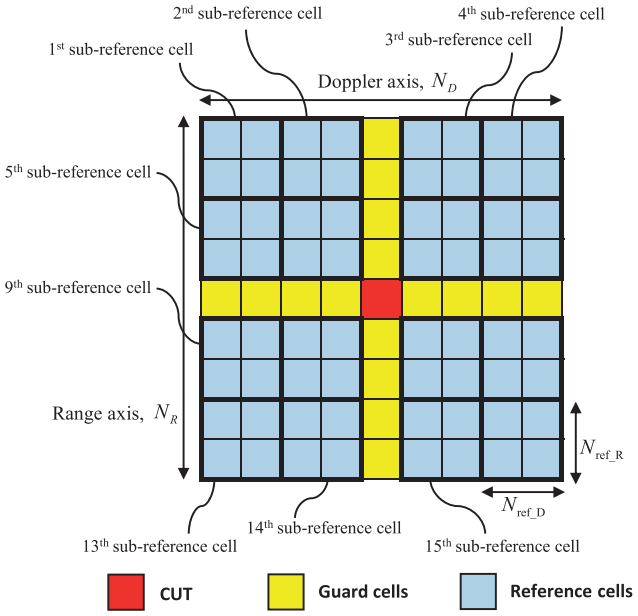

FIGURE 3. The shape of the two-dimensional window of the OSS-CFAR detector.

III. OSS-CFAR DETECTOR

In this section, we described the detection scheme and the false alarm rate of the proposed OSS-CFAR detector. The OSS-CFAR detector consists of three procedures: (1) definition of sub-reference cells, (2) estimation of the background level for each sub-reference cell, (3) calculation of the detection threshold by selecting one of the estimated background levels of the sub-reference cells. Details of the OSS-CFAR detector are described in the following subsections. In addition, the computational complexity of the OSS-CFAR detector is analyzed and compared with that of the conventional CFAR detectors.

A. DETECTION SCHEME OF THE OSS-CFAR

The shape of the two-dimensional window of the OSS-CFAR detector is provided in Fig. 3. The red cell is the CUT, the yellow cells are guard cells, and the blue cells are reference cells. The bold lines in the figure indicate the boundary of the sub-reference cells. There are 16 sub-reference cells, and all of these sub-reference cells contain the same number of cells. The reason the number of cells in the sub-reference cells is the same is to ensure that the same number of samples are used to estimate the background level of each sub-reference cell. In the range Doppler map, cells with the same range and the same Doppler as the CUT are set as the guard cells as shown in Fig. 3. This is to ensure that the range and Doppler sidelobe signals of the target in the CUT do not affect the estimation of the background level. This setting of the guard cells can reduce the effect of the sidelobe signals of a target in the CUT

when estimating the background level, so the accuracy of the background level estimation can be improved. The number of cells in the m-th sub-reference cell N_{REF_m} is as follows.

$$N_{REF_m} = N_{\text{ref\_R}} \times N_{\text{ref\_D}} \tag{17}$$

$$N_{\text{ref\_R}} = \frac{N_R - 1}{4}, N_{\text{ref\_D}} = \frac{N_D - 1}{4} \tag{18}$$

where $N_{\text{ref\_R}}$, $N_{\text{ref\_D}}$, N_R, and N_D are shown in Fig. 3 and m denotes the sub-reference cell number as follows.

$$m = 1, 2, \cdots, 16 \tag{19}$$

The background level of each sub-reference cell is estimated as follows.

$$\beta_m = \sum_{i,j \in REF_m} X(i,j) \tag{20}$$

where REF_m denotes the area of the m-th sub-reference cell.

We can set the estimated background levels $\{\beta_1, \beta_2, \cdots, \beta_{16}\}$ to form a new sequence in ascending order, denoted by $\{\beta_{(1)}, \beta_{(2)}, \cdots, \beta_{(16)}\}$.

$$\{\beta_1, \beta_2, \cdots, \beta_{16}\} \rightarrow \{\beta_{(1)}, \beta_{(2)}, \cdots, \beta_{(16)}\} \tag{21}$$

where

$$\beta_{(p)} \leq \beta_{(q)} \text{ when } p \leq q \tag{22}$$

The η-th background level of the ordered list is called the η-th ordered statistic of the OSS-CFAR detector. In the OSS-CFAR detector, the η-th background level was selected as the representative of the estimated background level, and the detection threshold is

$$T_{\text{OSS}} = \alpha_\eta \beta_{(\eta)} \tag{23}$$

where α_η denotes the scale factor, as described in the following subsection.

B. FALSE ALARM RATE OF THE OSS-CFAR

In this subsection, the false alarm rate of the OSS-CFAR detector is derived. If there is no target signal, the power of each range Doppler cell $X(i,j)$ is assumed to be independent and identically distributed (i.i.d.) samples of an exponential distribution denoted by (1). Because multiplying each range Doppler cell by any non-zero value has no effect on the detection probability and the false alarm rate in the proposed algorithm, each range Doppler cell $X(i,j)$ can be normalized by dividing by $2\sigma^2$ for convenience, which is the same manner as [11]. In this case, the PDF of $X(i,j)$ is given by,

$$P_X(x) = e^{-x} \tag{24}$$

The summation of powers in the m-th sub-reference cell, β_m, is i.i.d. samples of an Erlang distribution [21]. If we denote $y = \beta_m$, its PDF $P_Y(y)$ and cumulative distribution function (CDF) $F_Y(y)$ are given by,

$$P_Y(y) = \frac{y^{(N_{REF_m}-1)} e^{-y}}{(N_{REF_m} - 1)!} \tag{25}$$

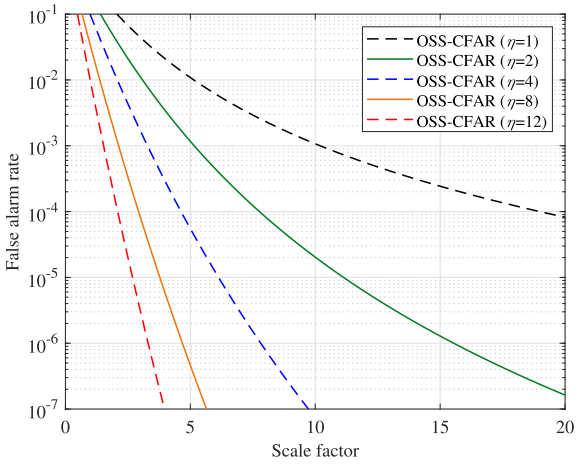

FIGURE 4. False alarm rates of the OSS-CFAR detector according to scale factor when the number of cells in the sub-reference cell N_{REF_m} is 4.

$$F_Y(y) = 1 - e^{-y} \sum_{q=0}^{N_{REF_m}-1} \frac{y^q}{q!} \tag{26}$$

$\beta_{(\eta)}$ is defined as the η-th ordered statistic of the i.i.d. random variable set $\{\beta_1, \beta_2, \cdots, \beta_{16}\}$. If we denote $z = \beta_{(\eta)}$, using [22], its PDF $P_Z^\eta(z)$ is given by,

$$P_Z^\eta(z) = \frac{M!}{(M-\eta)!(\eta-1)!} [F_Y(z)]^{\eta-1} [1 - F_Y(z)]^{M-\eta} P_Y(z) \tag{27}$$

where M is the number of sub-reference cells, which is 16 in Fig. 3.

The false alarm rate of the OSS-CFAR detector, $P_{\text{fa,OSS}}$, is given by the following expression, where X_{CUT} is the power of the CUT. To calculate the false alarm rate, it is assumed that there is only noise in the CUT as well as in the reference cells.

$$\begin{aligned} P_{\text{fa,OSS}} &= \int_0^\infty \Pr[X_{\text{CUT}} \geq \alpha_\eta \beta_{(\eta)}] P_Z^\eta(z)\ \mathrm{d}z \\ &= \int_0^\infty \left(\int_{\alpha_\eta z}^\infty P_X(x)\,\mathrm{d}x \right) P_Z^\eta(z)\ \mathrm{d}z \\ &= \int_0^\infty e^{-\alpha_\eta z} P_Z^\eta(z)\ \mathrm{d}z \end{aligned} \tag{28}$$

By substituting (25) and (27) into (28), $P_{\text{fa,OSS}}$ is obtained as below.

$$\begin{aligned} P_{\text{fa,OSS}} &= \frac{M!}{(M-\eta)!(\eta-1)!} \int_0^\infty e^{-\alpha_\eta z} \\ &\quad \cdot [F_Y(z)]^{\eta-1} [1 - F_Y(z)]^{M-\eta} P_Y(z)\ \mathrm{d}z \\ &= \frac{M!}{(M-\eta)!(\eta-1)!(N_{REF_m}-1)!} \int_0^\infty e^{-(\alpha_\eta+1)z} \\ &\quad \cdot z^{N_{REF_m}-1} [F_Y(z)]^{\eta-1} [1 - F_Y(z)]^{M-\eta}\,\mathrm{d}z \end{aligned} \tag{29}$$

As can be seen in (29), $P_{\text{fa,OSS}}$ depends only on the parameters related to M, N_{REF_m}, η, and the scale factor α_η. Therefore, the false alarm rate of the OSS-CFAR detector is independent of the power parameters. Based

TABLE 1. Comparison of computational complexity.

	Additions	Multiplications	Comparisons
CA-CFAR	N	–	–
SOCA-CFAR	N	–	1
GOCA-CFAR	N	–	1
OS-CFAR	–	–	$O(N \log_2 N)$
OSS-CFAR	N	–	$O(M \log_2 M)$

N: the number of the reference cells, M: the number of sub-reference cells.

on (26) and (29), $P_{\text{fa,OSS}}$ versus the scale factor α_η can be numerically calculated. For example, when the number of cells in the sub-reference cell N_{REF_m} is 4, the results are shown in Fig. 4. As a larger η is used, fewer false alarms occur with the same scale factor α_η. This is because the larger the η value is, the larger the estimated background level selected for the detection threshold.

C. COMPUTATIONAL COMPLEXITY

The computational complexity of the CFAR detectors is important in the radar system because of the real-time processing and implementation of the system. In this subsection, we analyzed the computational complexity of the OSS-CFAR detector and of the conventional CFAR detectors. Since the detection threshold of the CFAR detectors is a scale factor α times the estimated background level β, we only considered the computational complexity for calculating the estimated background level β.

We used big O notation, $O(\cdot)$, for analysis of the computational complexity. The comparison of the computational complexity of the CFAR detectors is shown in Table 1. In Table 1, N denotes the number of reference cells and M denotes the number of sub-reference cells. The CA-CFAR detector needs only N additions. The SOCA-CFAR and the GOCA-CFAR detectors need N additions and one comparison operation. Since the OS-CFAR and the OSS-CFAR detectors use a sorting algorithm, it is necessary to know the computational complexity of the sorting algorithm in order to analyze that of the OS-CFAR and the OSS-CFAR detectors. Since most sorting algorithms cannot perform better than $O(K \log_2 K)$ (on average) when sorting K samples [23], we assume that the sorting algorithm needs on average $O(K \log_2 K)$ comparison operations when sorting K samples. Therefore, the OS-CFAR and the OSS-CFAR detectors need $O(N \log_2 N)$ and $O(M \log_2 M)$ comparison operations, respectively.

In the proposed OSS-CFAR detector, the number of sub-reference cells M was set as 16. The number of the reference cells N is normally larger than the number of sub-reference cells M. Thus, the computational complexity of the OSS-CFAR detector is lower than that of the OS-CFAR detector, but higher than that of the CA-, SOCA-, and GOCA-CFAR detectors. Since the computational complexity of the OS-CFAR detector increases dramatically as the reference window size increases, whereas the computational complexity of the OSS-CFAR detector increases linearly as the reference window size increases, the OSS-CFAR detector achieves higher efficiency at the same performance level.

TABLE 2. Reference window size and guard cell size of CFAR detectors for multiple target situation simulations.

CA-, SOCA-, GOCA-, OS-CFAR		OSS-CFAR
Reference window size, N_R, N_D	Guard cell size, N_{GR}, N_{GD}	Reference window size, N_R, N_D
9	3	9

IV. SIMULATION RESULTS AND ANALYSIS

In this section, we compared the detection performance in multiple target situations and false alarm rate at the clutter edge of the OSS-CFAR detector with that of the conventional CFAR detectors using computer simulations.

A. DETECTION PERFORMANCE IN MULTIPLE TARGET SITUATIONS

In this subsection, two multiple target scenarios were simulated on the range Doppler map, and the detection performances of the OSS-CFAR detector and the conventional CFAR detectors were investigated. Multiple target situations usually occur when two or more targets are located close together on the range Doppler map. In this case, due to interfering targets, the measured background level is larger than the actual background level. This masking effect causes degradation of the detection performance of the conventional CFAR detectors.

Scenario 1: We generated a 100 by 100 range Doppler map (total 10,000 cells) with an exponentially distributed background, and several independent targets were randomly located on this range Doppler map. The expected power levels of these targets were set equal in each scenario, and the detection performance was analyzed while increasing the signal-to-clutter ratio (SCR) from 8 dB to 30 dB. To make it more realistic, the radar cross section (RCS) fluctuation model of the targets was modeled as a Swerling case I using Swerling target models [24]– [26] in each iteration.

Scenario 2: In the window of the CFAR detectors as shown in Fig. 1 and Fig. 3, we randomly located several independent interfering targets with interference-to-clutter ratios (ICR) of 20 dB in the reference cells. The detection performance was analyzed while increasing the target power of the CUT from 8 dB to 30 dB SCR. As in Scenario 1, the RCS fluctuation model of the interfering targets and the target in the CUT were modeled as a Swerling case I.

In Scenario 1, for all cells on the range Doppler map, detection was performed using the CFAR detectors, and the detection probabilities were calculated using the detection results and location information of the targets. A total of 10^5 Monte Carlo trials were performed for Scenario 1.

In Scenario 2, detection was performed only in the CUT, and the detection probabilities were calculated for each CFAR detector. A total of 10^7 Monte Carlo trials were performed for Scenario 2.

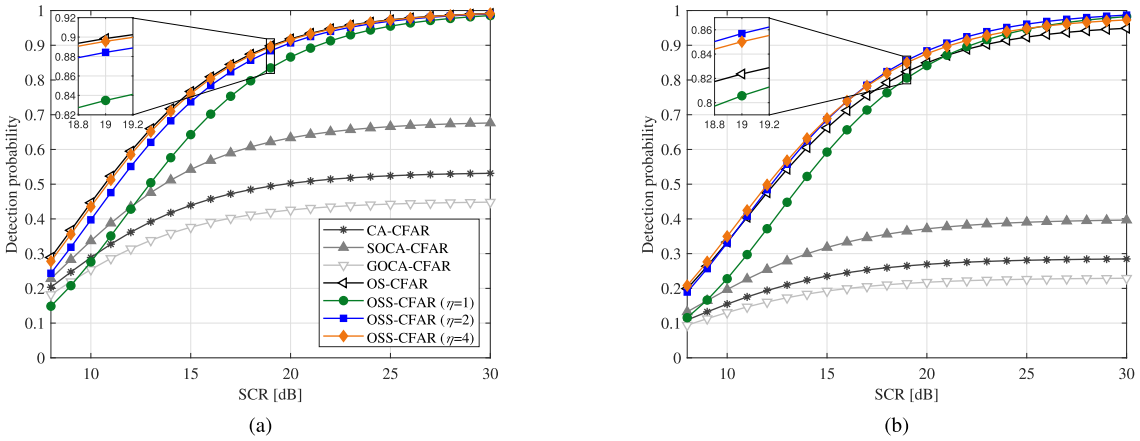

FIGURE 5. Detection probabilities in Scenario 1 for several independent targets: (a) 1,000, (b) 2,000.

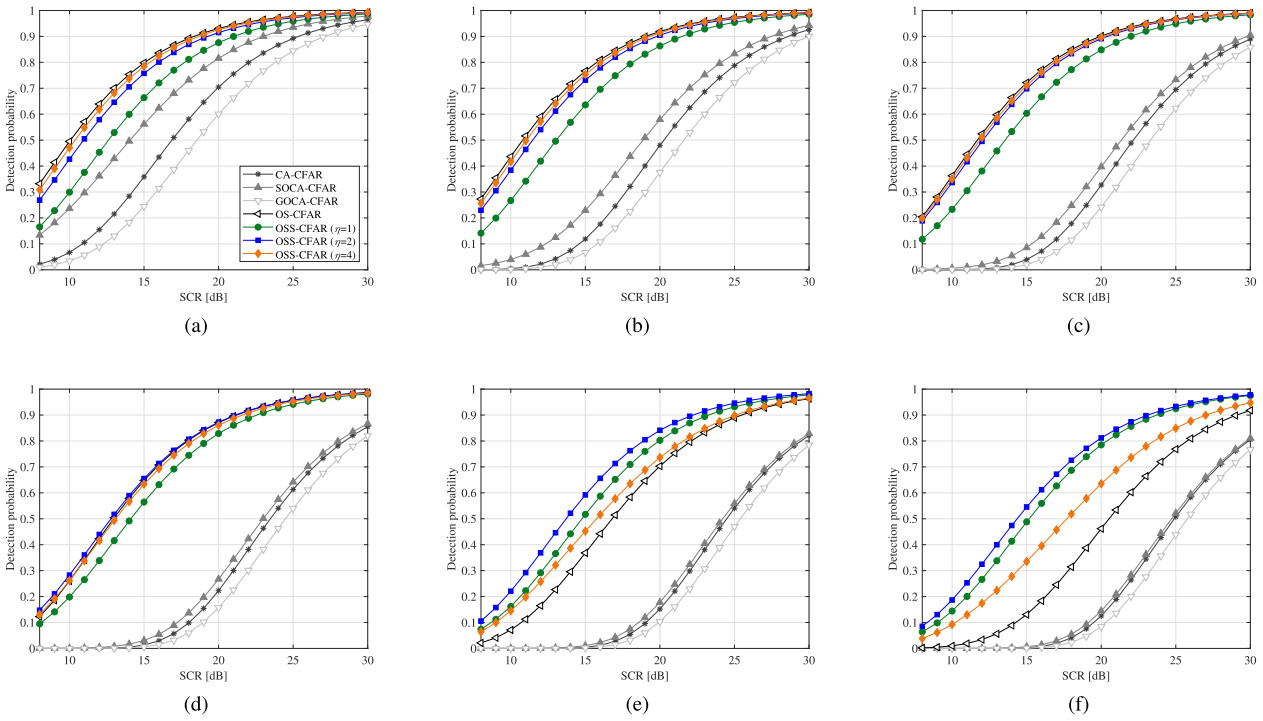

FIGURE 6. Detection probabilities in Scenario 2 for several independent interfering targets: (a) 3, (b) 7, (c) 11, (d) 15, (e) 19, (f) 21.

The range and Doppler size of the reference window N_R, N_D and the range and Doppler size of the guard cell for the conventional CFAR detectors N_{GR}, N_{GD} for multiple target situation simulations are as shown in Table 2. The desired false alarm rate was 10^{-3}. The background level representative value k of the OS-CFAR detector was set to $3N/4$ without loss of generality.

The detection probabilities with the 1,000 and 2,000 targets in Scenario 1 (generates 10% and 20% targets in the range Doppler map, respectively) are shown in Fig. 5(a) and Fig. 5(b), respectively. In both cases, the SOCA-, CA-, and GOCA-CFAR detectors exhibit performance degradation due to the masking effect. Since the SOCA-, CA-, and GOCA-CFAR detectors use minimum-selection, average, and maximum-selection schemes, respectively, the performance also degrades in the order of SOCA-, CA-, and GOCA-CFAR. The OS-CFAR and the OSS-CFAR detectors show good performance compared to the SOCA-, CA-, and GOCA-CFAR detectors. In Fig. 5(b), the OSS-CFAR detector shows better performance than the OS-CFAR detector owing to the serious masking effect as the number of targets increases.

The detection probabilities with the 3, 7, 11, 15, 19, and 21 interfering targets with ICR of 20 dB in Scenario 2 are shown in Fig. 6(a), 6(b), 6(c), 6(d), 6(e), and 6(f), respectively. In Fig. 6(a)–6(d), 3–15 interfering targets with ICR of 20 dB

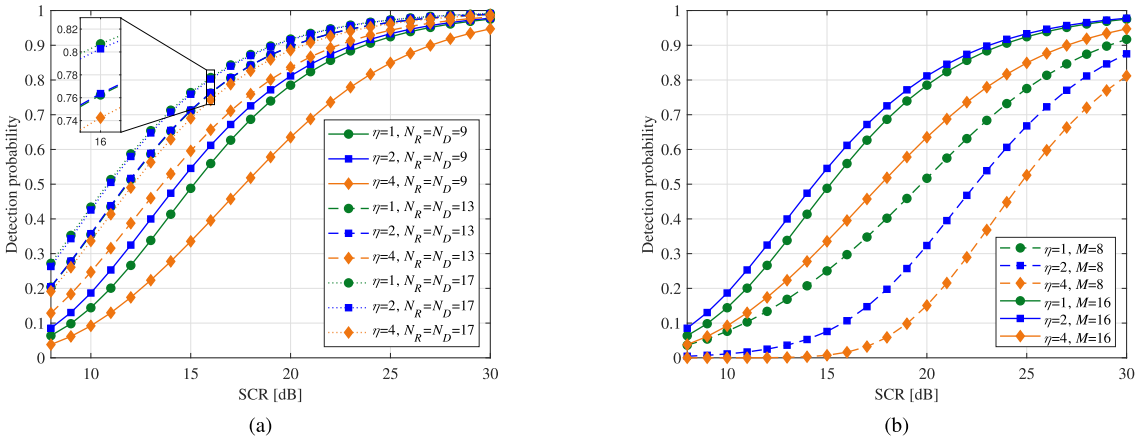

FIGURE 7. Detection probabilities of the OSS-CFAR detector with 21 interfering targets with ICR of 20 dB in Scenario 2 for different parameters (a) $N_R = N_D = 9$, 13, and 17 cases with $M = 16$, (b) $M = 8$ and 16 cases with $N_R = N_D = 9$.

are simulated. The OS-CFAR and the OSS-CFAR detectors provide good detection performances. However, the CA-, SOCA-, and GOCA-CFAR detectors exhibit performance degradation as the number of interfering targets increases due to the serious masking effect. In order to demonstrate the robustness of the OSS-CFAR detector to the high number of interfering targets, 19 and 21 interfering targets are simulated. In Fig. 6(e), 19 interfering targets with ICR of 20 dB are simulated. The detection performance of the OS-CFAR detector degraded compared to that of the OSS-CFAR detector because the value $N - k$ in the OS-CFAR detector, which is an acceptable number of interfering targets, is smaller than the number of interfering targets. In this case, $N - k = 72 - 54 = 18$, while the number of interfering targets is 19. As a result, the detection performance of the OS-CFAR detector is expected to degrade. In order to achieve good performance in multiple target situations, the OS-CFAR detector requires prior information about the number of interfering targets in the reference cells, but the OSS-CFAR detector does not require prior information about that. Therefore, the OSS-CFAR detector achieves robust detection performance without prior information in practical multiple target situations. In Fig. 6(f), 21 interfering targets with ICR of 20 dB are simulated. The detection performances of the OS-CFAR, CA-CFAR, SOCA-CFAR, and GOCA-CFAR detectors are degraded due to the masking effect. However, the OSS-CFAR detector still has better detection performance than the other detectors.

From the results in Fig. 5 and Fig. 6, it can be seen that the OSS-CFAR detector has the best performance in multiple target situations with a low computational complexity. In particular, overall, the OSS-CFAR detector with parameter η of 2 shows the best performance. Therefore, we recommend setting the parameter η to 2 in practical multiple target situations.

Since the detection performance of the OSS-CFAR detector depends on the parameters N_R, N_D, and M, we analyzed the detection probabilities with 21 interfering targets with ICR of 20 dB in Scenario 2 for different parameters N_R, N_D, and M, as shown in Fig. 7. The desired false alarm rate was 10^{-3}. In Fig. 7(a), $N_R = N_D = 9$, 13, and 17 cases with $M = 16$ are simulated. The detection probabilities of the OSS-CFAR detector increase as N_R and N_D increase. With the increase in the N_R and N_D, the corresponding detection probabilities increase because the powers of the interfering targets can be better averaged. That is, the effectiveness of the interfering targets is reduced as N_R and N_D increase. However, when N_R and N_D increase, the number of samples to be averaged increases, which may extend the computation time. Therefore, N_R and N_D should be appropriately selected. In Fig. 7(b), $M = 8$ and 16 cases with $N_R = N_D = 9$ are simulated. When N_R and N_D are fixed, the number of cells in each sub-reference cell increases as M decreases. Accordingly, since more interfering targets are included in each sub-reference cell, the estimated background level increases, thereby lowering the detection probability. As a result, in multiple target situations, a sufficiently large M value must be set. Nevertheless, since the computational complexity increases as M increases, an appropriate value should be given for M. Considering the trade-off between the detection performance and the computational complexity, we recommend setting M to 16 in practical multiple target situations.

B. FALSE ALARM RATE AT THE CLUTTER EDGE

In this subsection, the clutter edge was simulated and the false alarm rates of the CFAR detectors were investigated. This situation often occurs between the clutter region and the noise region. We assume that the power of the clutter and noise region is exponentially distributed with different mean powers. Given the different statistics of the adjacent regions, the samples in the reference cells are no longer i.i.d. if the samples with different mean power levels are involved simultaneously. At the clutter edge, the false alarm rate decreases if the CUT is located in a low power window, and the false alarm rate increases if it is located in a high power window. In general, the occurrence of false alarms in the high power cells can be problematic to radar performance. In this case,

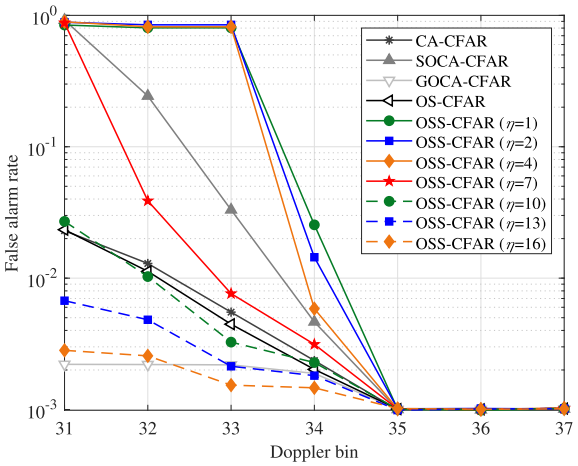

FIGURE 8. False alarm rates in the clutter edge.

the CFAR detectors have higher rates of false alarms unless appropriate signal processing methods are employed [19]. Therefore, in this subsection, the false alarm rate is analyzed in the clutter edge cells which have the higher power.

In this scenario, $[31 \times 60]$ range Doppler cells are generated for each iteration. The left-side cells ($[31 \times 30]$) and the right half cells ($[31 \times 30]$) are assumed to have different mean power levels. In this case, it is assumed that the left-side cells have lower power than the right half cells by 20 dB. The CFAR detection is performed on the 31st–37th Doppler cells, which are the clutter edge cells with the higher power between two different clutter regions. A total of 10^7 Monte Carlo trials were performed.

Fig. 8 shows the false alarm rates in the clutter edge with the reference window size and guard cell size (as in Table 2) for the desired false alarm rate of 10^{-3}. The results show that the false alarm rate of the SOCA-CFAR detector increases significantly at the clutter edge; the CA-CFAR and the OS-CFAR detector are slightly increased; the GOCA-CFAR detector works robustly. The false alarm rates of the OSS-CFAR detector vary for different parameters of η. The false alarm rate of the OSS-CFAR detector with $\eta = 1, 2, 4$, and 7 are significantly increased for the SOCA-CFAR detector. However, as the parameter η increases, the false alarm rate decreases.

Obviously, the OSS-CFAR detector with a larger η has better false alarm rate. However, the OSS-CFAR detector with a smaller η has better detection performance in multiple target situations. Since there is a trade-off between detection performance in multiple target situations and the false alarm rate at the clutter edge, it is necessary to select appropriately the parameter η according to the required performance. In practical scenarios, the detection probability of multiple targets is important for situational awareness, as ground and sea targets are often dense. In particular, in the case of military radar applications, since the missed detection of enemy targets is directly related to the threat to our forces, increasing the detection performance in multiple target situations is more important than reducing the occurrence of the false alarm rate at the clutter edge. Therefore, it is suggested to choose the smaller parameter η.

TABLE 3. Parameters of the experimental radar.

Parameter	Value
Carrier frequency	X-band
Range resolution	30 m
Doppler resolution	75.12 Hz
Pulse width	27 μs
Pulse repetition interval (PRI)	208 μs
Pulse repetition frequency (PRF)	4807 Hz
Number of pulses	64
Position of radar	On the aircraft in the East Sea, Republic of Korea
Date collection date	December 4, 2020

TABLE 4. Position information and SCR of real and simulated targets in Fig. 11(b).

	Range bin	Doppler bin	SCR [dB]	Feature
T1	567	28	37.4	real
T2	574	29	28.5	real
T3	584	29	34.5	real
T4	602	28	29.1	real
T5	589	27	32.5	simulated
T6	554	30	32.3	simulated
T7	593	30	33.8	simulated
T8	576	26	34.6	simulated
T9	577	29	34.7	simulated
T10	594	27	32.5	simulated

V. EXPERIMENTAL RESULTS AND ANALYSIS

In this section, we investigated the detection performances of the OSS-CFAR detector and the conventional CFAR detectors using the experimental data collected in the East Sea (Republic of Korea) on December 4, 2020. The experimental radar was mounted on the ramp door of a military transport aircraft (Lockheed Martin C-130 Hercules) and operated in the East Sea with four real targets (fishing boats with corner reflectors, T1–T4), as shown in Fig. 9 and Fig. 10 [27]. The direction of the radar antenna beam was opposite to the direction of flight, as shown in Fig. 9(a) and Fig. 10. The distance between the targets and the velocity of the targets in Fig. 10 were about 500 m and 8–12 m/s, respectively. The experimental radar operates in X-band and includes pulse compression mode and Doppler processing mode with compensation for the aircraft velocity. The range resolution and the Doppler resolution are 30 m and 75.12 Hz, respectively. The detailed parameters of the experimental radar are provided in Table 3.

A single snapshot of the range Doppler map from the collected experimental data is shown in Fig. 11(a). In the figure, there are four real targets from T1 to T4 with sea clutter. To simulate a more severe multiple target situation, we added six simulated targets (T5–T10) to this range Doppler map as shown in Fig. 11(b). In order to simulate more realistically, the power levels of the simulated targets were randomly set.

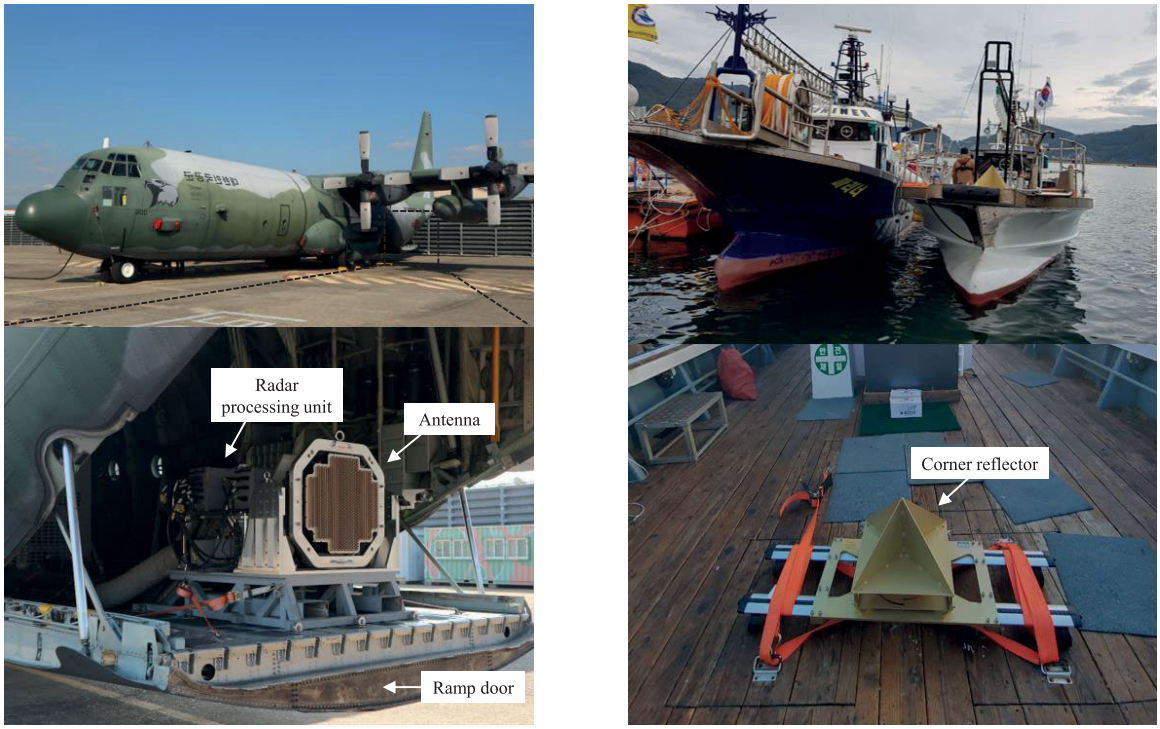

FIGURE 9. Experiment setup: (a) Military transport aircraft and experimental radar, (b) Fishing boat with corner reflector.

TABLE 5. Detection results of experimental data with simulated targets.

	Target number									
	T1	T2	T3	T4	T5	T6	T7	T8	T9	T10
OSS-CFAR($\eta = 1$)	◯	◯	◯	◯	◯	◯	◯	◯	◯	◯
OSS-CFAR($\eta = 2$)	◯	◯	◯	◯	◯	◯	◯	◯	◯	◯
OSS-CFAR($\eta = 4$)	◯	◯	◯	◯	◯	◯	◯	◯	◯	◯
OS-CFAR	◯	×	◯	◯	◯	◯	×	◯	◯	◯
SOCA-CFAR	◯	×	◯	◯	◯	◯	×	◯	◯	◯
GOCA-CFAR	◯	×	◯	◯	◯	×	×	◯	×	◯
CA-CFAR	◯	×	◯	◯	◯	×	×	◯	×	◯

T1–T4: real targets, T5–T10: simulated targets.
◯: detected, ×: missed.

That is, they were similar to the values of the real targets, and the power shapes in the range Doppler map of the simulated targets were simulated the same as for the real targets. The position information and SCR of the real and simulated targets in Fig. 11(b) are shown in Table 4.

Detection results of the experimental data with additional simulated targets are shown in Table 5. The reference window size and the guard cell size of the CFAR detectors were set in Table 2, and the background level representative value k of the OS-CFAR detector was $3N/4$. The desired false alarm rate was 10^{-3}.

The circle in Table 5 denotes that the corresponding target is detected correctly, and "×" denotes that the corresponding target was missed. The results show that the CA-CFAR and GOCA-CFAR detectors performed the worst in multiple target situations due to the masking effect. The two

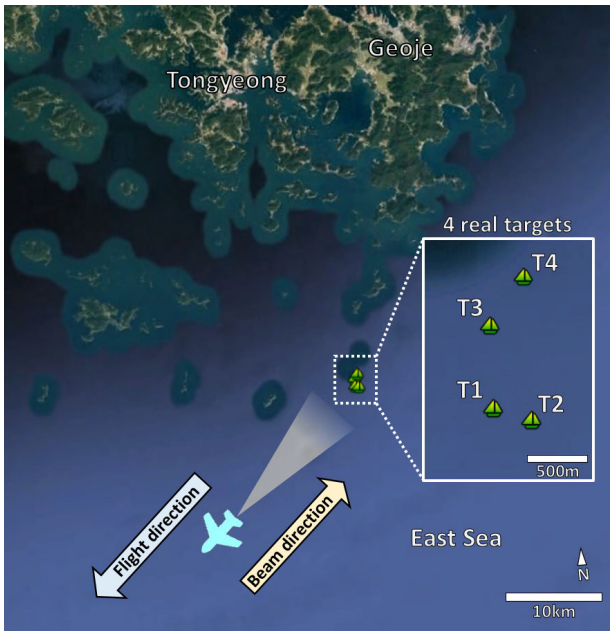

FIGURE 10. Experimental data acquisition of four real targets with real sea clutter.

detected only six out of ten targets. The OS-CFAR and SOCA-CFAR detectors exhibited relatively robust detection performance in multiple target situations, but missed two targets: T2 (weak power and many other targets nearby) and

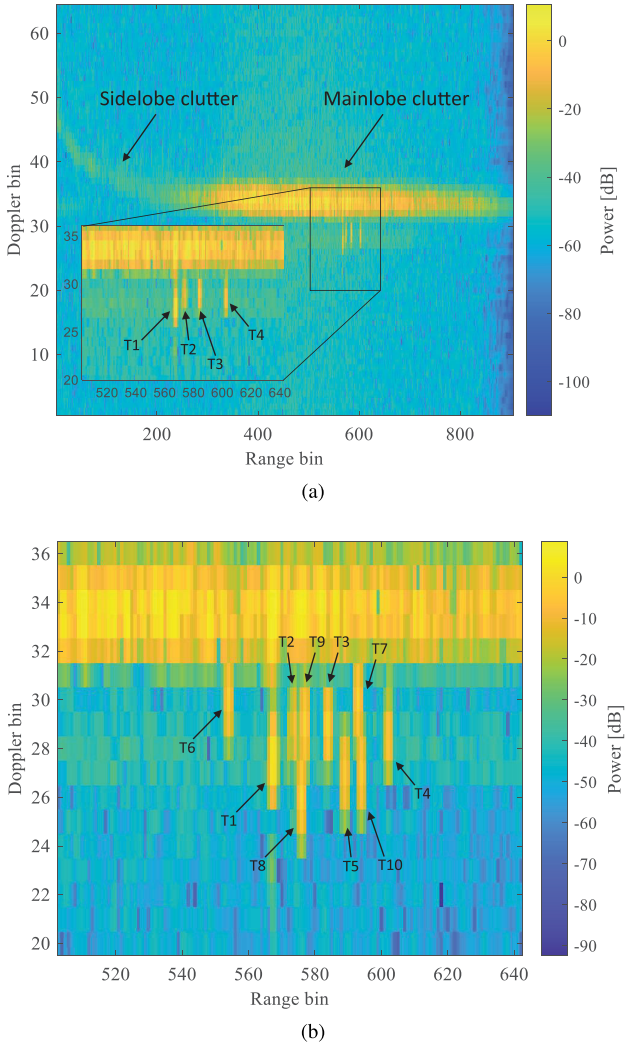

FIGURE 11. Snapshot of range Doppler map from collected experimental radar data with (a) Four real targets (T1–T4), (b) Four real targets (T1–T4) plus six simulated targets (T5–T10).

T7 (near the mainlobe clutter of the sea clutter). The proposed OSS-CFAR detector achieved the best performance in multiple target situations with sea clutter as it detected all targets with different parameters of η. In other words, it was confirmed that the OSS-CFAR detector works well even in the sea clutter that follows a K-distribution rather than an exponential distribution. Therefore, the proposed OSS-CFAR detector is robust in practical multiple target situations with sea clutter.

VI. CONCLUSION

In this paper, we proposed a robust CFAR detector with ordered statistic of sub-reference cells in multiple target situations and the clutter edge. Estimating the background level for each sub-reference cell and setting guard cells with the same range and the same Doppler as the CUT, the accuracy of the background level estimation can be improved since the range and Doppler sidelobe signals of the target in the CUT do not affect estimation of the background level. In addition, the computational complexity is low compared to that of the OS-CFAR detector. This is achieved using the ordered statistic of sub-reference cells since it only needs to sort by the number of sub-reference cells.

The OS-CFAR detector requires prior information about the number of interfering targets in order to remove all interfering targets from the reference cells. The OSS-CFAR detector, in contrast, does not require prior information about that. Therefore, the OSS-CFAR detector achieves robust detection performance without prior information in practical multiple target situations.

For verification of the proposed OSS-CFAR detector results, Monte Carlo computer simulations were performed in multiple target situations and at the clutter edge. As a result, the detection performance of the OSS-CFAR detector is improved in multiple target situations compared to the conventional CFAR detectors with low computational complexity. Moreover, experimental results show the effectiveness and robustness of the OSS-CFAR detector when compared to conventional CFAR detectors in multiple target situations with sea clutter. At the clutter edge, the OSS-CFAR detector with appropriate parameters achieves acceptable false alarms compared to the conventional CFAR detectors. Therefore, using the OSS-CFAR detector with appropriate parameter η in multiple target situations will help detect multiple radar targets and recognize situations because it can improve detection performance in practical scenarios.

REFERENCES

[1] Y. Li, Y. Wei, B. Li, and G. Alterovitz, "Modified Anderson-darling test-based target detector in non-homogenous environments," *Sensors*, vol. 14, no. 9, pp. 16046–16061, Aug. 2014.

[2] D. Tao, S. N. Anfinsen, and C. Brekke, "Robust CFAR detector based on truncated statistics in multiple-target situations," *IEEE Trans. Geosci. Remote Sens.*, vol. 54, no. 1, pp. 117–134, Jan. 2016.

[3] W. Wang, R. Wang, R. Jiang, H. Yang, and X. Wang, "Modified reference window for two-dimensional CFAR in radar target detection," *J. Eng.*, vol. 2019, no. 21, pp. 7924–7927, Nov. 2019.

[4] R. G. Zefreh, M. R. Taban, M. M. Naghsh, and S. Gazor, "Robust CFAR detector based on censored harmonic averaging in heterogeneous clutter," *IEEE Trans. Aerosp. Electron. Syst.*, vol. 57, no. 3, pp. 1956–1963, Jun. 2021.

[5] X. Meng, "Performance evaluation of RQ non-parametric CFAR detector in multiple target and non-uniform clutter," *IET Radar, Sonar Navigat.*, vol. 14, no. 3, pp. 415–424, Mar. 2020.

[6] X. Meng, "Rank sum nonparametric CFAR detector in nonhomogeneous background," *IEEE Trans. Aerosp. Electron. Syst.*, vol. 57, no. 1, pp. 397–403, Feb. 2021.

[7] W. Liu, J. Liu, C. Hao, Y. Gao, and Y.-L. Wang, "Multichannel adaptive signal detection: Basic theory and literature review," *Sci. China Inf. Sci.*, vol. 65, no. 2, Feb. 2022, Art. no. 121301.

[8] M. A. Richards, *Fundamentals of Radar Signal Processing*, 1st ed. New York, NY, USA: McGraw-Hill, 2005.

[9] H. M. Finn and R. S. Johnson, "Adaptive detection mode with threshold control as a function of spatial sampled clutter level estimates," *RCA Rev.*, vol. 29, no. 3, pp. 414–464, Sep. 1968.

[10] P. P. Gandhi and S. A. Kassam, "Analysis of CFAR processors in nonhomogeneous background," *IEEE Trans. Aerosp. Electron. Syst.*, vol. AES-24, no. 4, pp. 427–445, Jul. 1988.

[11] M. Weiss, "Analysis of some modified cell-averaging CFAR processors in multiple-target situations," *IEEE Trans. Aerosp. Electron. Syst.*, vol. AES-18, no. 1, pp. 102–114, Jan. 1982.

[12] V. G. Hansen and J. H. Sawyers, "Detectability loss due to 'greatest of' selection in a cell-averaging CFAR," *IEEE Trans. Aerosp. Electron. Syst.*, vol. AES-16, no. 1, pp. 115–118, Jan. 1980.
[13] H. Rohling, "Radar CFAR thresholding in clutter and multiple target situations," *IEEE Trans. Aerosp. Electron. Syst.*, vol. AES-19, no. 4, pp. 608–621, Jul. 1983.
[14] W. Zhou, J. Xie, G. Li, and Y. Du, "Robust CFAR detector with weighted amplitude iteration in nonhomogeneous sea clutter," *IEEE Trans. Aerosp. Electron. Syst.*, vol. 53, no. 3, pp. 1520–1535, Jun. 2017.
[15] L. Ye, F. Jian, Y. Yang, W. Zhang, Q. Yang, and Q. Chen, "Weighted distance iteration matrix CFAR detector in sea clutter," *IET Radar, Sonar Navigat.*, vol. 14, no. 10, pp. 1631–1639, Oct. 2020.
[16] L. Wang, D. Wang, and C. Hao, "Intelligent CFAR detector based on support vector machine," *IEEE Access*, vol. 5, pp. 26965–26972, 2017.
[17] J. Zhao, R. Jiang, X. Wang, and H. Gao, "Robust CFAR detection for multiple targets in K-distributed sea clutter based on machine learning," *Symmetry*, vol. 11, no. 12, p. 1482, Dec. 2019.
[18] N. R. Subramanyan and A. Vengadarajan, "Robust variability index CFAR for non-homogeneous background," *IET Radar, Sonar Navigat.*, vol. 13, no. 10, pp. 1775–1786, Oct. 2019.
[19] W. Zhou, J. Xie, K. Xi, and Y. Du, "Modified cell averaging CFAR detector based on Grubbs criterion in non-homogeneous background," *IET Radar, Sonar Navigat.*, vol. 13, no. 1, pp. 104–112, Jan. 2019.
[20] J. T. Rickard and G. M. Dillard, "Adaptive detection algorithms for multiple-target situations," *IEEE Trans. Aerosp. Electron. Syst.*, vol. AES-13, no. 4, pp. 338–343, Jul. 1977.
[21] A. Papoulis and S. U. Pillai, *Probability, Random Variables and Stochastic Processes*, 4th ed. New York, NY, USA: McGraw-Hill, 2002.
[22] E. J. Gumbel, *Statistics of Extremes*. New York, NY, USA: Columbia Univ. Press, 1958.
[23] T. H. Cormen, C. E. Leiserson, R. L. Rivest, and C. Stein, *Introduction to Algorithms*, 3rd ed. Cambridge, MA, USA: MIT Press, 2009.
[24] P. Swerling, "Probability of detection for fluctuating targets," *IRE Trans. Inf. Theory*, vol. IT-6, no. 2, pp. 269–308, Apr. 1960.
[25] F. E. Nathanson, *Radar Design Principles*, 1st ed. New York, NY, USA: McGraw-Hill, 1991.
[26] M. I. Skolnik, *Introduction to Radar Systems*, 3rd ed. New York, NY, USA: McGraw-Hill, 2001.
[27] *Google Earth Pro V7.3.3.7786. (Date of Original Imagery: Dec. 14, 2015), Image Copyright: 2021 CNES/Airbus, 2021 TerraMetrics*, Data Copyright: SIO, NOAA, U.S. Navy, NGA, GEBCO, Maxar Technol., Westminster, CO, USA, 2021.

TAEHEE JEONG received the B.S. degree in electronics and computer engineering from Hanyang University, Seoul, Republic of Korea, in 2009, and the M.S. degree in electrical engineering from the Pohang University of Science and Technology (POSTECH), Pohang, Republic of Korea, in 2011. He is currently pursuing the Ph.D. degree in electrical engineering with the Korea Advanced Institute of Science and Technology (KAIST), Daejeon, Republic of Korea.

Since 2011, he has been a Senior Researcher with Agency for Defense Development (ADD), Daejeon, Republic of Korea. His current research interests include airborne pulsed Doppler radar signal processing, surface moving target detection, and modern radar detection theory.

SUNGYEONG PARK received the B.S. and M.S. degrees in electrical engineering from the Korea Advanced Institute of Science and Technology (KAIST), Daejeon, Republic of Korea, in 2014 and 2016, respectively.

Since 2016, he has been a Senior Researcher with Agency for Defense Development (ADD), Daejeon. His current research interests include airborne pulsed Doppler radar signal processing and modern radar detection theory.

JEONG-WOOK KIM received the B.S. degree in electronics engineering from Pusan National University (PNU), Busan, Republic of Korea, in 2018, and the M.S. degree in electrical engineering from the Korea Advanced Institute of Science and Technology (KAIST), Daejeon, Republic of Korea, in 2020, where he is currently pursuing the Ph.D. degree in electrical engineering.

His current research interests include active phase array antenna systems, wireless power charging systems, invisible antennas, radar system design, and signal processing.

JONG-WON YU (Member, IEEE) received the B.S., M.S., and Ph.D. degrees in electrical engineering from the Korea Advanced Institute of Science and Technology (KAIST), Daejeon, Republic of Korea, in 1992, 1994, and 1998, respectively.

From 1995 to 2000, he was with Samsung Electronics, Suwon, Republic of Korea. From 2000 to 2001, he was with Wide Telecom, Seoul, Republic of Korea. From 2001 to 2004, he was with Telson Electronics, Seoul. In 2004, he joined KAIST, as an Assistant Professor, where he is currently a Professor with the School of Electrical Engineering. His current research interests include microwave millimeter wave circuits (hybrid), wireless power transfer, wireless near-field communication systems, and radio frequency identification/ubiquitous sensor networks (USNs).